Minerals Engineering 120 (2018) 66–74

Contents lists available at ScienceDirect

Minerals Engineering

journal homepage: www.elsevier.com/locate/mineng

Effect of ball milling on the carbon sequestration efficiency of serpentinized peridotites

Ioannis Rigopoulos[a,*], Andreas Delimitis[b,1], Ioannis Ioannou[c], Angelos M. Efstathiou[d], Theodora Kyratsi[a]

[a] Department of Mechanical and Manufacturing Engineering, University of Cyprus, 1678 Nicosia, Cyprus
[b] Chemical Process & Energy Resources Institute (CPERI), Centre for Research & Technology Hellas (CERTH), 6th km Charilaou – Thermis Road, GR-57001 Thermi, Thessaloniki, Greece
[c] Department of Civil and Environmental Engineering, University of Cyprus, 1678 Nicosia, Cyprus
[d] Department of Chemistry, Heterogeneous Catalysis Lab, University of Cyprus, 1678 Nicosia, Cyprus

ARTICLE INFO

Keywords:
Ball milling
Carbon capture and storage (CCS)
CO_2 chemisorption
CO_2-TPD
Harzburgite
Mineral carbonation
Ultramafic rocks

ABSTRACT

Mineral carbonation has been suggested as a safe carbon capture and storage (CCS) strategy for the mitigation of climate change. This study investigates the effect of ball milling on the CO_2 sequestration capacity of peridotites, which are among the most promising readily available lithologies for CCS on the Earth's surface. A partially serpentinized harzburgite from the Troodos ophiolite (Cyprus) was subjected to different degrees of ball milling to produce nanoscale ultramafic powders with enhanced CO_2 uptake. The optimum ball milling conditions were found (16 h of wet ball milling with 50 wt% ethanol as process control agent) through CO_2 chemisorption followed by temperature-programmed desorption (CO_2-TPD) experiments. The results clearly showed that the CO_2 uptake of the initial rock material was increased by a factor of 4.5 after ball milling. Detailed characterization of the unmilled and ball-milled samples indicated that this enhancement is mainly attributed to (i) the reduction of particle size down to the nanoscale range and (ii) the structural disordering of the constituent Mg-silicate minerals due to mechanical deformation.

1. Introduction

The concentration of atmospheric CO_2 has been increased from a pre-industrial level of 280 ppm to 404 ppm in 2016 (NOAA-ESRL, 2017), primarily due to the widespread use of fossil fuels (Ciais et al., 2013; Keeling et al., 1995; Sawyer, 1972; Siegenthaler and Oeschger, 1987). This abrupt increase is considered to be the main reason for the observed global climate change (IPCC, 2005; Kuo et al., 1990), which seems to be largely irreversible on human timescales (Solomon et al., 2009). Thus, significant efforts have been made to develop efficient carbon capture and storage (CCS) technologies (e.g. Gislason and Oelkers, 2014; Lackner et al., 1995; Matter et al., 2016; Michael et al., 2010; Wilson et al., 2014). The recent COP21 Paris Agreement sets out a global action plan in order to put the world on track and avoid future dangerous climate changes by limiting the global warming to well below 2 °C above the pre-industrial levels (UNFCCC, 2016).

Mineral carbonation is a CCS technology that includes the conversion of CO_2 into carbonate minerals (Lackner et al., 1995; Oelkers et al., 2008; Olajire, 2013; Power et al., 2013; Sanna et al., 2014; Seifritz, 1990). It comprises the chemical reaction of rocks containing Mg and/or Ca-silicate minerals with CO_2 to form carbonate minerals, such as magnesite ($MgCO_3$), calcite ($CaCO_3$) and dolomite ($CaMg(CO_3)_2$), which are stable over geologic time. Therefore, this carbon sequestration approach minimizes the risk of leakage and thus facilitates long-term and safe storage (e.g. Gislason and Oelkers, 2014; Matter and Kelemen, 2009; Matter et al., 2016; Seifritz, 1990). Peridotites are among the main sources of forsteritic olivine, which is the most promising mineral for carbon sequestration (O'Connor et al., 2005; Oelkers et al., 2008). The main carbonation reactions of peridotites are described by the following Eqs. (1)–(3):

$$\underset{\text{Forsterite}}{Mg_2SiO_4} + 2CO_2 \rightarrow 2\underset{\text{Magnesite}}{MgCO_3} + \underset{\text{Silica}}{SiO_2} \quad (1)$$

$$\underset{\text{Enstatite}}{MgSiO_3} + CO_2 \rightarrow \underset{\text{Magnesite}}{MgCO_3} + \underset{\text{Silica}}{SiO_2} \quad (2)$$

* Corresponding author.
E-mail addresses: rigopoulos.ioannis@ucy.ac.cy (I. Rigopoulos), andreas.delimitis@uis.no (A. Delimitis), ioannis@ucy.ac.cy (I. Ioannou), efstath@ucy.ac.cy (A.M. Efstathiou), kyratsi@ucy.ac.cy (T. Kyratsi).
[1] Currently at the Department of Mechanical and Structural Engineering and Materials Science, University of Stavanger, 4036 Stavanger, Norway.

https://doi.org/10.1016/j.mineng.2018.02.011
Received 17 October 2017; Received in revised form 7 February 2018; Accepted 18 February 2018
Available online 24 February 2018
0892-6875/

$$\underset{\text{Serpentine}}{Mg_3Si_2O_5(OH)_4} + 3CO_2 \rightarrow \underset{\text{Magnesite}}{3MgCO_3} + \underset{\text{Silica}}{2SiO_2} + 2H_2O \quad (3)$$

The mineralization of CO_2 can be performed either *in situ*, by injecting CO_2 into ultramafic or mafic rocks (e.g. Matter and Kelemen, 2009; Matter et al., 2016), or *ex situ* in industrial reactors, after mining and crushing/grinding the rock material (e.g. Bodénan et al., 2014; Gerdemann et al., 2007; Rigopoulos et al., 2016a). *Ex situ* carbonation could provide a potential solution to sequester CO_2 from small to medium capacity emitters, where geological storage is not a viable option (Sanna et al., 2014). The major challenges of *ex situ* mineral carbonation are the scale of mining operations, the high energy consumption and the slow reaction kinetics (Gerdemann et al., 2007). Several studies have been performed to speed up the *ex situ* carbonation reactions by: (i) grinding/milling the rock materials, (ii) increasing the temperature, and (iii) dissolving the rock material in various solutions (e.g. Declercq et al., 2013; Haug et al., 2010; Li and Hitch, 2016a; Rigopoulos et al., 2015a, 2015b, 2016a, 2016b). In addition, many works have focused on the *ex situ* carbon mineralization of industrial wastes (e.g. mine tailings, construction waste), which could contribute to the reduction of atmospheric CO_2 concentrations and result in a number of economic benefits for many industries (Li and Hitch, 2017a; Power et al., 2013; Sanna et al., 2014; Wilson et al., 2014). An additional advantage of such a process is that it could reduce the hazardous nature of certain wastes, such as asbestos minerals (Bobicki et al., 2012). Emphasis should also be placed on the fact that the final products of mineral carbonation could be used by the construction industry as additives in order to render the whole approach more economically viable.

During the last decade, several studies focused on the application of milling techniques to olivine (Baláž et al., 2008; Haug et al., 2010; Kleiv and Thornhill, 2006, 2016; Li and Hitch, 2016a; Turianicová et al., 2013). However, only a few works have performed experiments using partially altered olivine-rich rocks (i.e. basalts, dunites) (Rigopoulos et al., 2015a, 2016a, 2017), which are much more abundant on the Earth's surface compared to pure olivine. In addition, the effect of mechanical activation on the carbon sequestration efficiency of ultramafic rocks/mine waste materials has been thoroughly studied by Li and Hitch (2016b, 2016c, 2017a, 2017b).

The aim of this paper is to assess the effect of the ball milling process on the CO_2 uptake of partially serpentinized harzburgites, which are among the most important rocks for the mineralization of CO_2 due to their relatively high content in forsterite-rich olivine. Although harzburgite is less reactive compared to dunite, it can be found in significantly larger quantities worldwide. In the framework of this study, we performed several ball milling experiments to produce ultrafine powders of high surface areas and determine the optimum ball milling conditions for harzburgites. The experiments were performed using a planetary ball mill, since this type of mill is commonly used for the production of ultrafine powders. The results obtained were then used to explain the effect of ball milling on the CO_2 chemisorption (uptake) over these nanoscale ultramafic materials.

2. Materials and methods

2.1. Sample selection, preparation and characterization

In the present study, a sample of harzburgite was collected from the western part of the Troodos mantle section (north of Mount Olympos; Fig. 1) for the preparation of nanoscale ultramafic materials with enhanced CO_2 uptake.

The Troodos ophiolite complex (Fig. 1) is the most intact ophiolite worldwide. It was formed in a supra-subduction zone environment around 92–90 Ma ago (Cenomanian-Turonian), based on U-Pb isotopic dating of plagiogranites (Mukasa and Ludden, 1987; Robertson, 2002; Robinson and Malpas, 1990). Its mantle section is divided into two units (Batanova and Sobolev, 2000). The eastern unit consists of spinel lherzolite with dunite bodies and zones of clinopyroxene-bearing harzburgite, while the western unit is principally composed of clinopyroxene-poor harzburgite and dunite. Above these mantle rocks, cumulate ultramafic and mafic lithotypes are found, which are cut by gabbroic intrusives; the upper massive gabbros locally include small plagiogranite bodies. Upwards, the sheeted dyke complex trends nearly N-S (Robertson, 2002). The overlying pillow lavas are traditionally divided into the "Lower" and "Upper" Pillow Lava units (LPL and UPL) (Gass and Smewing, 1973).

The mineralogical and textural characteristics of the studied rock sample were determined by petrographic analysis of a representative

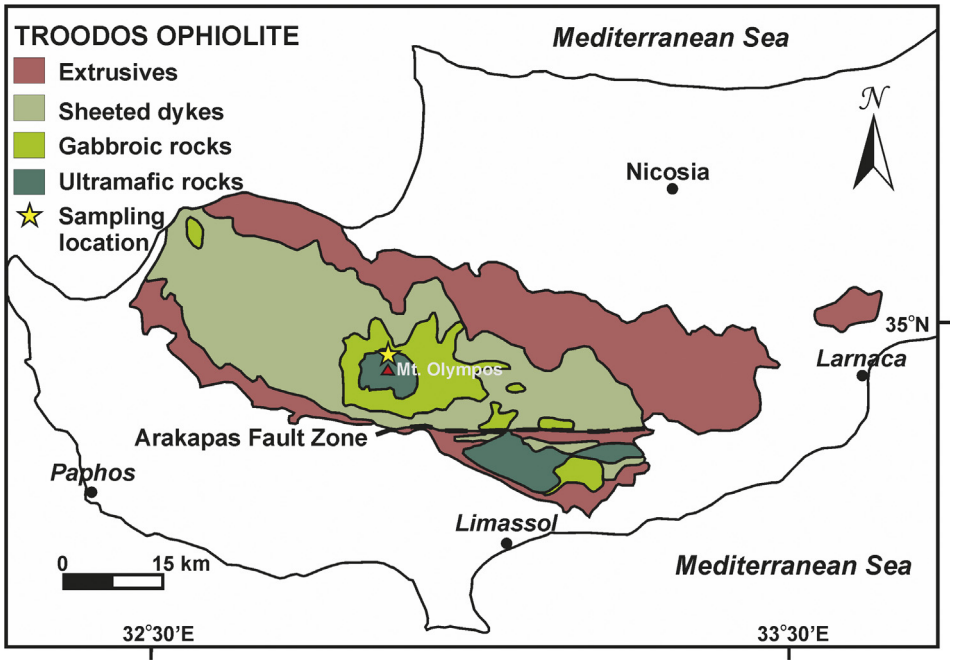

Fig. 1. Simplified geological-sampling map of the Troodos ophiolite, modified after Pearce and Robinson (2010).

thin section using a polarizing microscope. The sample was then ground with a stainless steel pulverizer and sieved to obtain the 104–150 μm size fraction. This particular fraction was chosen to avoid internal mass transport resistances during CO_2 chemisorption (uptake) and the subsequent CO_2-TPD measurements (Section 2.6). A portion of this size fraction was used as starting material, while the remainder was ball-milled to further reduce its grain size. The non-ball milled size fraction is henceforth referred to as "unmilled".

2.2. Ball milling

Ball milling was performed using a Fritsch Pulverisette 6 planetary mono mill. The optimum milling conditions for ultramafic rocks in terms of CO_2 uptake were applied, based on the results of previous studies (Rigopoulos et al., 2016a). The harzburgite was wet-milled in an 80 mL tungsten carbide bowl using ethanol as process control agent (PCA). Although water is the most commonly used milling liquid, previous experiments have shown that ethanol results in milled ultramafic rocks with substantially higher CO_2 uptakes (Rigopoulos et al., 2016a). The ball-to-powder mass ratio was 20:1 w/w, the liquid-to-powder mass ratio was 1:2, and the rotation speed was 300 rpm. The process was carried out using 30 tungsten carbide balls with a 10 mm diameter. Tungsten carbide bowl and balls were used to avoid possible contamination of the rock material, taking into account the high hardness of mantle lithologies. The ball milling process was automatically interrupted every 5 min for 5 min to avoid sample heating. This periodic interruption avoids phase transformations and reduces the evaporation of the PCA, especially during many hours of ball milling. After milling was complete, the recovered powder/ethanol slurry was allowed to dry overnight at room temperature. The milling conditions are summarized in Table 1.

2.3. Powder X-ray diffraction (PXRD)

The solids were characterized by powder X-ray diffraction (PXRD) using a Bruker D8 Advance system in order to identify the mineral crystal phases of the studied ultramafic samples and to investigate potential mineralogical transformations that might have occurred during the ball milling process. The analyses were carried out with a continual rotation of the sample and a step of 1°/min within the 3–80° 2θ angle range. The ICDD PDF 2 database was used for the qualitative identification of the constituent minerals.

2.4. Surface texture

A surface area and pore size analyzer (Micromeritics, model Gemini III) was used to determine the specific surface area ($m^2\,g^{-1}$), the specific pore volume ($cm^3\,g^{-1}$) and the average pore diameter (nm) of the studied rock materials by the BET method (adsorption of N_2 at 77 K) (measurement uncertainty: ± 5%). Each measurement was taken after the sample was outgassed in dry nitrogen flow at 250 °C for 2 h.

2.5. Electron microscopy

The unmilled and ball-milled materials were characterized using a JEOL, JSM-6610 LV scanning electron microscope (SEM), equipped with a BRUKER type QUANTAX 200 energy dispersive spectrometer (EDS). The effect of the ball milling process on the studied peridotite was determined using secondary electron images (SEI). EDS analyses were also performed in order to determine the chemical composition of the constituent minerals.

Samples for conventional TEM as well as high resolution transmission electron microscopy (HRTEM) observations were prepared by smoothly grinding the sample in high-purity ethanol using an agate pestle and mortar. A drop of the suspension was subsequently deposited onto a lacey C-film supported on a Cu grid and was allowed to evaporate under ambient conditions. A high resolution transmission electron microscope was used (JEOL 2011), operating at 200 kV with a point resolution of 0.23 nm and $C_s = 1.0$ mm. Chemical analysis was performed by energy-dispersive X-ray spectroscopy (EDXS). For this reason, the microscope is fitted with an INCAx-sight liquid nitrogen cooled EDXS detector with an ultrathin window. Processing of the spectra was accomplished using the INCA Microanalysis Suite software.

2.6. CO_2 chemisorption followed by temperature-programmed desorption (CO_2-TPD)

Temperature-programmed desorption (TPD) of CO_2 in He carrier gas was performed in a specially designed gas flow-system (Costa et al., 2000), in order to evaluate both the concentration (μmol g^{-1}) of adsorbed CO_2 on the basic sites of the material under study (oxygen anionic sites), and the distribution of strength of CO_2 adsorption due to the heterogeneity of the surface of the adsorbent material. The latter is related to the temperature of appearance of the CO_2 desorption rate maximum in the TPD trace (Efstathiou and Bennett, 1990).

The temperature of the samples under investigation (W = 0.7 g, unmilled and ball-milled samples) was initially increased to 500 °C under He gas flow and maintained at this temperature for approximately 1 h until the CO_2 background signal ($m/z = 44$ in He flow) in the mass spectrometer was reached. The feed was then switched to 5 vol % CO_2/He gas mixture (50 N mL min^{-1}) at 500 °C for 30 min, and the sample was cooled for about 1 h to 50 °C under that mixture. The initial chemisorption temperature used (i.e. 500 °C) was selected based on the optimum conditions determined by previous studies on ultramafic samples (Rigopoulos et al., 2016a). After the sample was cooled to 50 °C in the CO_2/He flow, the feed gas was switched to He flow for approximately 15 min, until no signal of CO_2 in He flow was detected in the mass spectrometer. The CO_2-TPD experiment was then conducted by increasing the temperature of the sample from 50 to 950 °C (rate of temperature increase, $\beta = 30$ °C/min). Calibration of the CO_2 signal ($m/z = 44$) of the mass spectrometer was carried out based on a certified calibration gas mixture of 985 ppm CO_2 in He diluent gas.

Table 1
Ball milling conditions and textural properties of the unmilled and ball-milled harzburgite samples.

	Ball milling conditions		Textural properties		
Sample code	Milling time (h)	Type of milling	BET ($m^2\,g^{-1}$)	Pore volume ($cm^3\,g^{-1}$)	Avg pore diameter (nm)
SM17	–	–	2.2	0.003	5.7
BM67	1 h	Wet (50 wt% Ethanol)	23.7	0.096	15.8
BM68	2 h	Wet (50 wt% Ethanol)	31.7	0.119	13.9
BM69	4 h	Wet (50 wt% Ethanol)	37.5	0.122	12.1
BM70	8 h	Wet (50 wt% Ethanol)	45.1	0.152	12.7
BM71	12 h	Wet (50 wt% Ethanol)	50.5	0.140	10.8
BM72	16 h	Wet (50 wt% Ethanol)	53.1	0.174	11.5
BM73	20 h	Wet (50 wt% Ethanol)	45.2	0.173	14.0

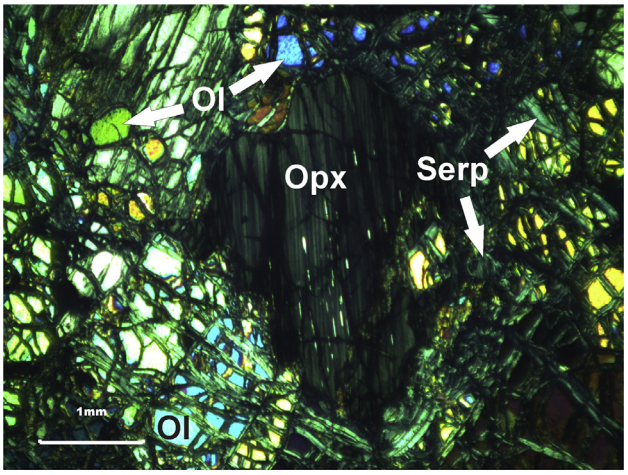

Fig. 2. Photomicrograph (crossed polars) of the harzburgite showing porphyroclastic texture (Ol: olivine, Serp: serpentine, Opx: orthopyroxene).

3. Results

3.1. Petrography

The harzburgite under study is a moderately serpentinized peridotite, showing mainly porphyroclastic and/or cataclastic texture (Fig. 2). Its primary mineralogical composition includes olivine (Fo_{90-92}) (~70%), orthopyroxene (enstatite) (> 25%) with exsolution lamellae of clinopyroxene (diopside), and minor Cr-spinel (~2–3%). Hydrothermal alteration has mainly resulted in the development of serpentine, as well as of smaller amounts of chlorite and talc. Locally, transgranular microcracks crosscut the rock as a result of brittle deformation.

3.2. Powder XRD (PXRD)

PXRD analyses indicated that the mineralogical composition of the harzburgite included forsterite, enstatite, antigorite, lizardite and chlorite (Fig. 3a). The results are in agreement with the data acquired during the petrographic analysis (see Section 3.1). PXRD patterns were also obtained for the ball-milled samples, showing that there is no mineralogical transformation due to the ball milling process. However, milling caused a substantial reduction in the intensity of all XRD peaks and led to the disappearance of some smaller peaks (compare Fig. 3a and b). These observations tend to become more obvious with increasing milling time, as demonstrated by the negative correlation between the ball milling duration and the ratio of maximum intensity to mean background intensity (see inset in Fig. 3b). The aforementioned suggest for the structural disordering of the constituent silicate minerals.

3.3. Surface texture

The specific surface area (BET, $m^2\,g^{-1}$), pore volume ($cm^3\,g^{-1}$) and average pore diameter (nm) of the unmilled and ball-milled samples are given in Table 1. Fig. 4 shows the variation of these textural parameters with increasing ball milling duration. During the first 2 h of ball milling, the specific surface area and pore volume showed an abrupt increase, followed by a smaller increase between 2 and 16 h. The maximum values of these textural parameters were acquired after 16 h of ball milling, while a reduction is observed after longer milling (Fig. 4a and b). The maximum pore diameter value was obtained after 1 h of ball milling; however, this textural parameter does not exhibit a clear trend with increasing ball milling time (Fig. 4c).

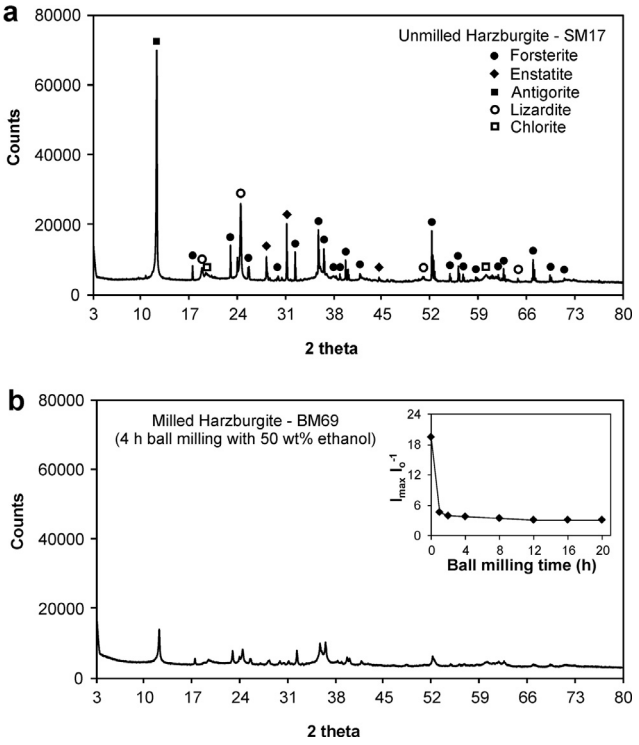

Fig. 3. Powder X-ray diffraction patterns of (a) the unmilled harzburgite and (b) the rock material after 4 h of ball milling with 50 wt% ethanol as PCA. Inset shows the relationship between the ball milling time (h) and the ratio of maximum intensity (I_{max}) to mean background intensity (I_o). The maximum intensity corresponds to the peak with the highest intensity in each PXRD pattern and the mean background intensity is the average of four background intensities.

3.4. Scanning electron microscopy (SEM)

SEM images were acquired from the unmilled and ball-milled harzburgite samples. The unmilled material has large and angular particles (Fig. 5a), the size of which corresponds to the aperture size of the sieves (104–150 μm) that were used to acquire the fraction of the starting rock material. The presence of serpentine (see Section 3.1), which belongs to the phyllosilicate subclass of minerals, has promoted the production of some flaky particles during the grinding process (see Fig. 5a). In addition, the particles of the unmilled material are usually covered by fine particles (Fig. 5a). In contrast, the particles of the ball-milled materials are substantially smaller, more rounded and uniform (Fig. 5b–d). Detailed observations showed that the particle size decreases with increasing ball milling time (compare Fig. 5b and c). Additionally, the ball-milled samples usually contain agglomerated powder particles, which are very frequent after many hours of ball milling (Fig. 5d).

3.5. Transmission electron microscopy (TEM and HRTEM)

TEM experiments were performed on the ball-milled harzburgite with the highest specific surface area and CO_2 uptake (sample BM72; see Tables 1 and 2), emphasizing on olivine, which is the dominant mineral phase. EDS point analysis results obtained from numerous areas of the sample indicated that the forsterite content in olivine crystals ranges between 90 and 92%. Additionally, EDS point analyses confirmed the presence of significant amounts of enstatite and antigorite.

Fig. 6a confirms the significant reduction of particle size to the nanoscale range due to mechanical deformation. In more detail, the majority of the particle sizes after the ball milling process ranges from 15 to 60 nm, while a few bigger particles were also detected (up to 470 nm). Furthermore, TEM observations revealed that the majority of

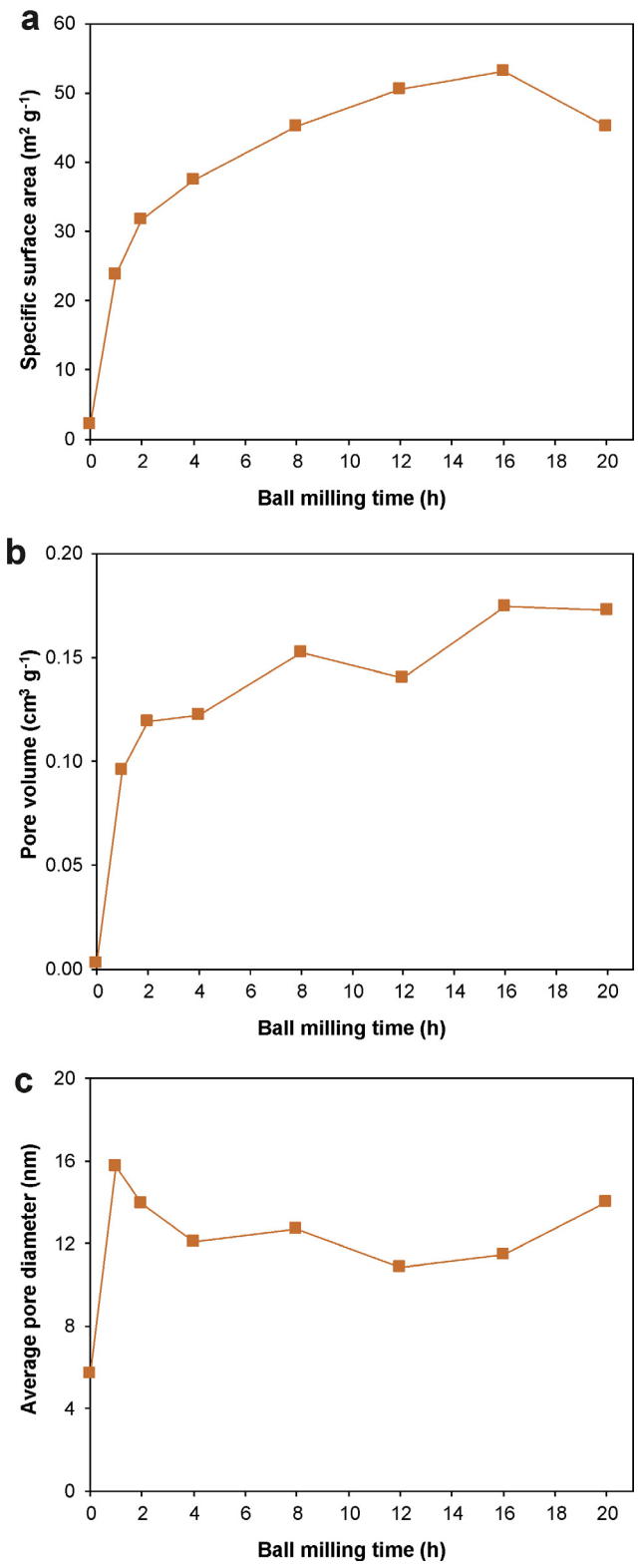

Fig. 4. (a) BET ($m^2\,g^{-1}$) specific surface area, (b) pore volume ($cm^3\,g^{-1}$) and (c) average pore diameter (nm) plotted versus the ball milling time (h).

the antigorite and enstatite particles were highly disordered to amorphous, implying that ball milling tends to disturb the crystal structure of the constituent minerals. As shown in Fig. 6b, antigorite was found as highly disordered and/or amorphous particles. The low resistance of serpentine to mechanical deformation is attributed to its low hardness (Li and Hitch, 2017b). In contrast, olivine crystals, which are significantly harder, were still highly crystalline after milling (Fig. 6c), as denoted by the selected area diffraction (SAD) pattern (see inset of Fig. 6c); this indicates their high resistance to mechanical deformation. Thorough observations revealed that the more disordered areas occur on the periphery of each individual olivine particle, while the interior often includes residual highly crystalline areas (as implied by the Moire fringes circled in Fig. 6d).

Additionally, detailed observations confirmed that quite a few particles are actually composed of smaller nanoparticles. This agglomeration was clearly revealed by complementary bright field (BF) and dark field (DF) images (Fig. 6e and f). Some of the primary nanocrystals forming the larger one can be seen in Fig. 6f. The sizes of these primary nanoparticles are quite small, ranging between 3 and 6 nm.

3.6. CO_2 chemisorption followed by TPD

CO_2 temperature-programmed desorption traces were acquired for the unmilled and ball-milled samples following the procedure described in Section 2.6. The concentration (in units of $\mu mol\,g^{-1}$ and $mg\,g^{-1}$) of the basic sites accommodating the desorbed CO_2 was estimated after integrating the respective CO_2 desorption trace (CO_2 concentration vs time) and considering the appropriate material balance for a flow reactor. For this estimation, the concentration of desorbed CO_2 at 950 °C (isothermal desorption) in He flow until no desorption of CO_2 had been detected was considered (not shown in Fig. 7).

The temperatures at which maximum desorption rates (T_{max}, °C) were observed and the total CO_2 uptake (or the equivalent desorbed amount) of the studied samples are summarized in Table 2. The estimated CO_2 uptake reflects the quantity of carbonate species formed on the surface of each sample during chemisorption from a 5 vol% CO_2/He gas mixture. The experimental results indicate that the unmilled sample has a potential, albeit limited, CO_2 adsorption capacity (sample SM17: 22.8 $\mu mol\,g^{-1}$; Table 2). After ball milling, the CO_2 uptake of the harzburgite has been substantially enhanced. The largest increase was detected after 16 h of milling (sample BM72: 103.4 $\mu mol\,g^{-1}$; Table 2).

In the unmilled harzburgite, the presence of different in strength surface basic sites is represented by three desorption peaks (peak maxima at 128, 677 and 817 °C), with the largest one appearing at 677 °C as shown in Fig. 7a. The peak intensities of the ball-milled samples are higher compared to the unmilled rock material. The highest temperature peak of the unmilled sample (T_{max} = 817 °C; Fig. 7a) shows a notable enhancement after ball milling (Fig. 7b–d). The intensity of this peak gradually increases with increasing ball milling time (compare Fig. 7b–d), suggesting that an increased ball milling duration promotes the formation of more strongly bound carbonate species. This is further supported by the presence of a new peak at even a higher temperature (T_{max} = 878 °C) after 16 h of ball milling (Fig. 7d). Furthermore, a new low-temperature desorption peak (T_{max} = 250 °C) appears after 1 h of ball milling (Fig. 7b). Contrary to the high-temperature peaks, the low-temperature ones (T_{max} = 128 and 250 °C) show only a slight enhancement with increasing ball milling time (compare Fig. 7b and d).

The correlation between the ball milling duration and the estimated CO_2 uptake of the studied rock materials (using a 5% CO_2/He gas mixture) confirms that ball milling substantially enhances the CO_2-adsorption capacity of serpentinized harzburgites (Fig. 8). As already mentioned, the maximum CO_2 uptake was recorded after 16 h of ball milling, inducing an increase of the CO_2-storage capacity by a factor of 4.5 compared to the unmilled sample (i.e. from 22.8 to 103.4 $\mu mol\,g^{-1}$). This increase is significantly faster during the first 4 h of milling, while it becomes notably smaller between 4 and 16 h of milling. As shown in Fig. 8, further ball milling results in a slight decrease of CO_2 uptake.

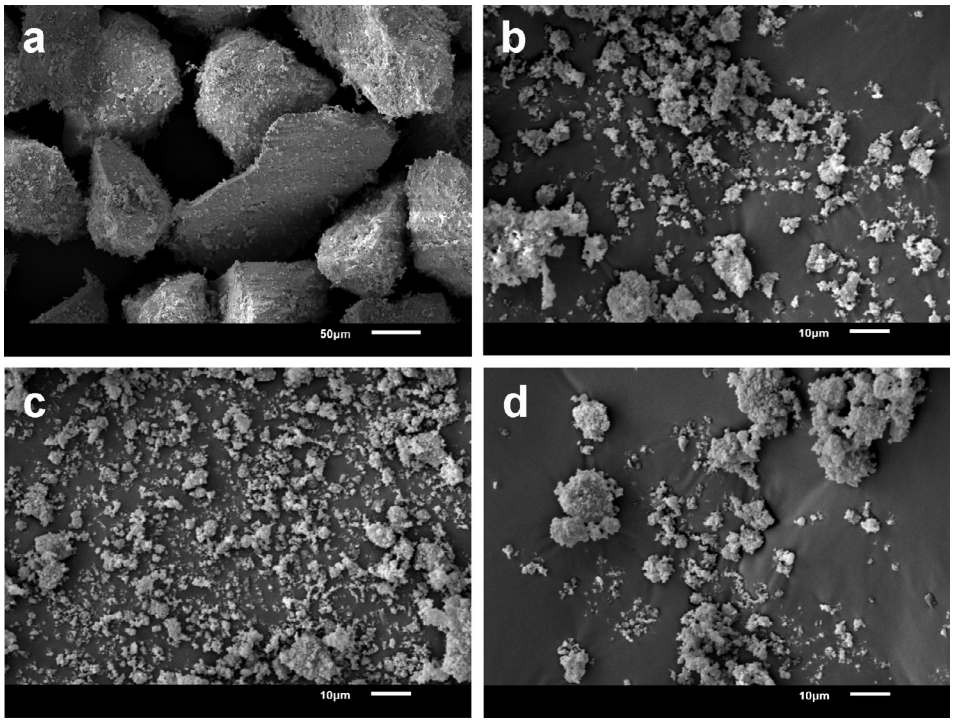

Fig. 5. SEM images of the harzburgite under study: (a) SM17 (unmilled material), (b) BM67 (ball-milled for 1 h), (c) BM72 (ball-milled for 16 h), (d) BM73 (ball-milled for 20 h). The magnification in Fig. 5a is significantly lower compared to that in Fig. 5b–d.

4. Discussion

The greatest challenge of *ex situ* carbonation is to accelerate the CO_2 adsorption kinetics of suitable rock materials in order to develop an efficient and economically viable CCS method (Gerdemann et al., 2007; Olajire, 2013; Sanna et al., 2014). The current work has investigated a method to enhance the CO_2 sequestration capacity of harzburgites, which are among the most abundant sources of divalent cations (i.e. Mg^{2+}, Fe^{2+}) that are essential for the carbonation process.

The ball milling process was applied to a partially serpentinized harzburgite in order to produce nanoscale ultramafic materials with enhanced CO_2 uptake. An initial substantial increase of specific surface area, pore volume and average pore diameter was observed due to the effect of ball milling (Fig. 4). These trends are well supported by SEM and TEM observations (Figs. 5 and 6), which show that the ball-milled samples contain notably smaller, more rounded and uniform particles compared to the unmilled rock. The main increase of specific surface area takes place during the first 4 h of ball milling (Fig. 4a). The maximum value of specific surface area was, nevertheless, reached after 16 h of milling, while a reduction was observed after additional milling. This reduction is assigned to the fact that a gradually increased proportion of agglomerated nanoparticles tends to be created after prolonged milling (Fig. 5d). Thorough TEM observations confirmed the reduction of the particle size to the nanoscale range (Fig. 6a), as well as the agglomeration of nanoparticles after many hours of ball milling. The increase of pore volume and mean pore diameter after milling are considered significant parameters for the rate of CO_2 uptake, since the diffusion rate within a porous structure becomes less important than the kinetics of CO_2 chemisorption and carbonation. Regarding mean pore diameter, it does not show a clear trend with increasing ball milling time. This is likely attributed to the altered character of the original harzburgite sample, which involves primary and secondary minerals of different resistance to mechanical deformation.

CO_2-TPD experiments indicated that the ball milling process can substantially improve the CO_2 sequestration capacity of harzburgites. The trend acquired between the duration of ball milling and the quantity of adsorbed CO_2 indicates a fast increase of the sequestered CO_2 during the first 4 h of ball milling (see Fig. 8). The maximum increase of CO_2 uptake was acquired after 16 h of ball milling, leading to an improvement by a factor of 4.5 compared to the unmilled rock (see Fig. 8; Table 2). A slight reduction of the amount of adsorbed CO_2 was observed after additional ball milling. This trend is very similar to the relationship between the ball milling duration and the specific surface area (Fig. 4a), suggesting that the increase of the number of surface basic sites that are responsible for the carbonation process is mainly attributed to the substantial increase of specific surface area caused by

Table 2
Peak maximum desorption temperatures (T_{max}) and amounts of adsorbed CO_2 (μmol g^{-1} or mg g^{-1}) (after chemisorption from 5 vol% CO_2/He) estimated from CO_2-TPD experiments for the unmilled and ball-milled harzburgite samples.

Sample code	T_{max1} (°C)	T_{max2} (°C)	T_{max3} (°C)	T_{max4} (°C)	T_{max5} (°C)	μmol CO_2 g^{-1}	mg CO_2 g^{-1}
SM17 (unmilled)	128	–	677	817	–	22.8	1.00
BM67 (milled: 1 h)	128	250	666	802	–	55.1	2.42
BM68 (milled: 2 h)	131	236	659	801	–	64.7	2.85
BM69 (milled: 4 h)	135	231	643	793	–	80.3	3.53
BM70 (milled: 8 h)	128	244	627	793	–	84.9	3.73
BM71 (milled: 12 h)	129	252	635	791	–	100.5	4.42
BM72 (milled: 16 h)	133	248	632	786	878	103.4	4.55
BM73 (milled: 20 h)	148	257	631	790	878	98.9	4.35

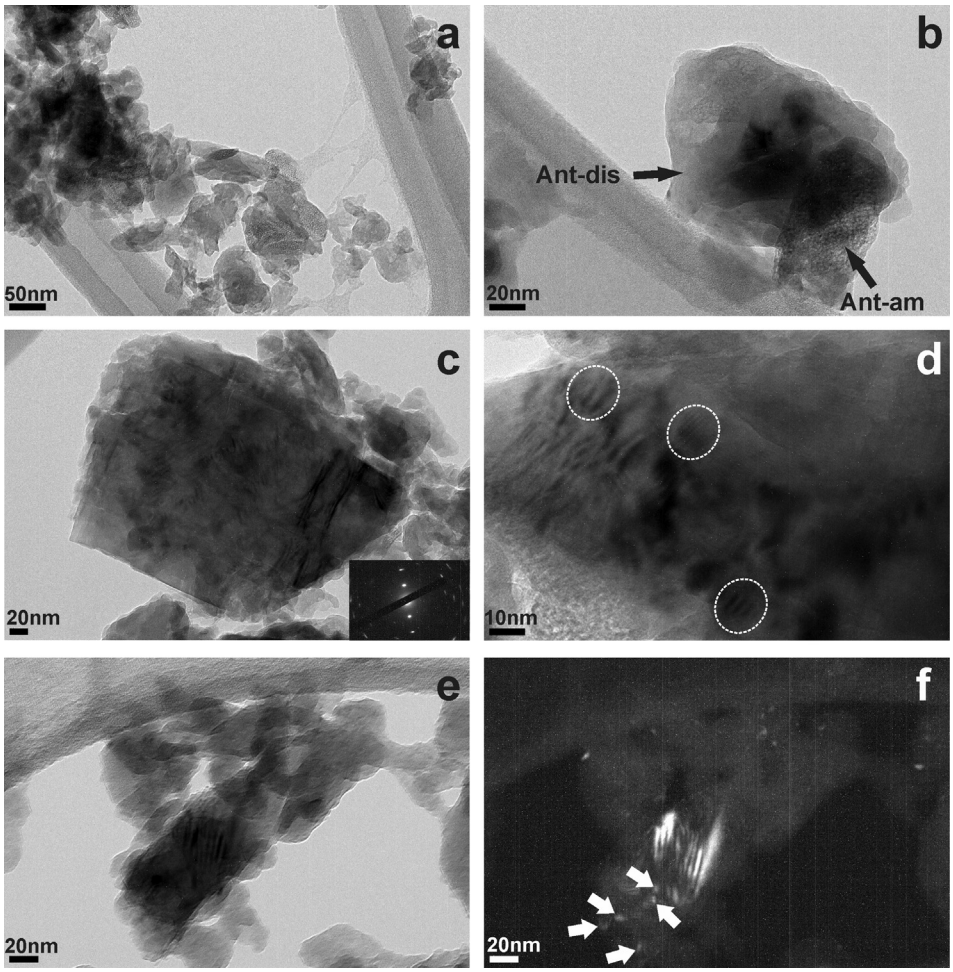

Fig. 6. TEM images of the ball-milled harzburgite with the highest specific surface area and CO_2 uptake (sample BM72), showing: (a) the reduction of particle size to the nanoscale range, (b) the presence of highly disordered (Ant-dis) and amorphous (Ant-am) antigorite, (c) the crystallinity of olivine particles, (d) the existence of highly crystalline areas in the interior of olivine particles; (e) BF image and (f) complementary DF image both depicting the agglomeration of nanocrystals during ball milling (see arrows).

the ball milling process. It is important to note that the sample with the highest CO_2 uptake also shows the highest pore volume (see Fig. 4b). This supports the idea that the ball milling process enhances the rate of mass transport of CO_2 within the porous structure of the rock material, thereby promoting the rate of chemisorption of CO_2. Additionally, the ball milling process creates many crystal defects, many of which comprise surface sites that promote the formation of carbonate-type species (CO_2 (g) + $O^{n-} \leftrightarrow CO_3^{n-}$) during CO_2 chemisorption. Although the formation of these carbonate species usually takes place on the surface of each nanoparticle, this surface carbonation is the first critical step prior to bulk carbonation. The aforementioned results are in agreement with similar studies in other ultramafic and mafic lithotypes (Rigopoulos et al., 2015a, 2015b, 2016a, 2016b). It is worth noting that an aqueous mineral carbonation scheme would lead to a substantially higher degree of carbonation (e.g. see Gerdemann et al., 2007; Kemache et al., 2016).

Furthermore, CO_2-TPD experiments clearly showed that the intensity of the highest temperature desorption peak, which occurs at 817 °C in the unmilled sample (see Fig. 7a), gradually increases with increasing ball milling duration (see Section 3.6). In addition, a new peak appears after 16 h of ball milling, at an even higher temperature (Fig. 7d). These observations indicate that the ball milling process promotes the formation of strongly bound carbonate species, thus eliminating the risk of later leakage of CO_2 back to the atmosphere and reducing the need for any monitoring program. The aforementioned are in line with the results of similar CO_2-TPD studies performed in waste materials from mafic rock quarries (Rigopoulos et al., 2016b).

The enhanced CO_2 uptake of harzburgite after ball milling is mainly attributed to the mechanical deformation of olivine ($Mg_{2-x}Fe_xSiO_4$), which is the most promising mineral for carbonation purposes (Li and Hitch, 2016a; Rigopoulos et al., 2016a). Although enstatite ($MgSiO_3$) is less reactive than olivine, it is considered that its CO_2 sequestration capacity has been considerably enhanced due to the ball milling process (see Rigopoulos et al., 2015b). Similarly, the reaction rates of serpentine ($Mg_3Si_2O_5(OH)_4$) with CO_2 are significantly lower compared to those between olivine and CO_2 (Gerdemann et al., 2007; Oelkers et al., 2008). However, the notably enhanced CO_2 uptake of harzburgites after ball milling suggests that the latter has also increased to some extent the ability of serpentine to sequester CO_2. A further substantial improvement could be achieved by removing the chemically bound H_2O from the lattice of serpentine via thermal pre-treatment; however, such a step would considerably increase the cost of the whole approach (Balucan and Dlugogorski, 2013; Dlugogorski and Balucan, 2014; O'Connor et al., 2005).

PXRD in combination with TEM studies showed that the ball-milled samples are composed of a large number of highly disordered or amorphous particles (see Figs. 3b and 6b). The substantial reduction of the PXRD peaks intensity with increasing ball milling time (see inset of Fig. 3b) suggests that ball milling modifies the crystal structure and morphology of the primary crystals present in the rock material, and thus the characteristics (number, density and strength) of the surface basic sites of the final nanoscale materials. The most remarkable decrease of the PXRD peaks intensity occurs within the first hour of ball milling, while further milling causes significantly smaller changes (see

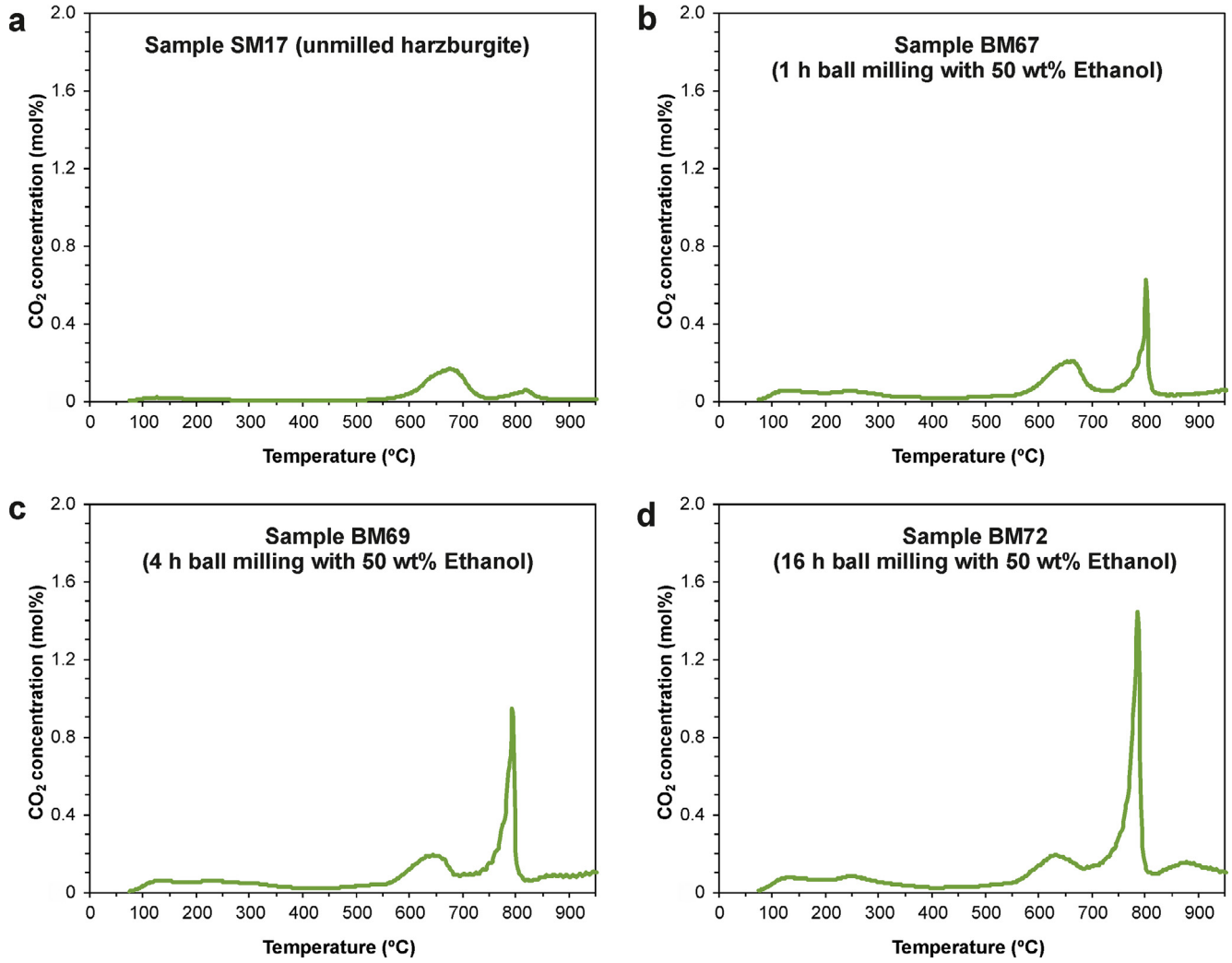

Fig. 7. CO_2 temperature-programmed desorption (TPD) traces obtained under He flow for (a) the unmilled material (SM17) and (b-d) representative ball-milled samples. Adsorption conditions: 5 vol% CO_2/He (50 N mL/min) at 500 °C for 30 min followed by cooling of the sample to 50 °C under the same gas mixture. Desorption conditions: Q_{He} = 50 N mL/min, β = 30 °C/min.

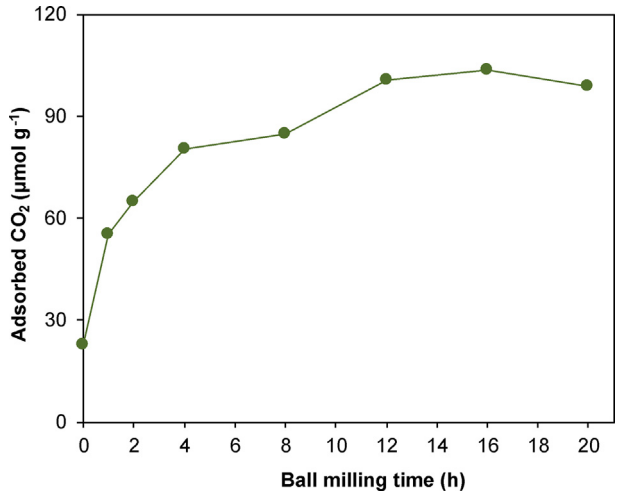

Fig. 8. Adsorbed CO_2 (μmol g^{-1}) versus ball milling time (h) for the unmilled harzburgite and the ball-milled rock materials.

inset of Fig. 3b). Detailed TEM observations revealed that the most disordered areas occur on the periphery of each individual particle, while the interior often includes residual highly crystalline areas. This indicates that some mineral particles (mainly olivine) partially retain their crystallinity, even after many hours of ball milling, due to their high hardness and in turn resistance to mechanical deformation. Previous studies have shown that a substantial enhancement of the carbonation reactions can be observed due to the presence of disordered Mg- and/or Ca-silicate minerals (Kleiv and Thornhill, 2006; Li and Hitch, 2016a; Munz et al., 2012; Rigopoulos et al., 2016b; Turianicová et al., 2013). In the current work, the structural disordering of the constituent Mg-silicate minerals is considered an additional reason for the enhanced CO_2 uptake after ball milling.

Despite the notably enhanced CO_2 uptake of harzburgite after ball milling, it should be mentioned that the energy costs required for the implementation of this carbonation method are considerably high. The overall carbon sequestration efficiency depends on the amount of CO_2 produced during mining, grinding/milling, transportation and carbonation of the material. Therefore, future studies should focus on the economic evaluation of this approach, the carbon sequestration efficiency of the whole methodology by using different types of mills, as well as on the potential carbonation of milled peridotites under lower temperatures. However, a main counter-advantage of this carbon sequestration plan is the abundance of partially serpentinized peridotites in several places around the world, thus eliminating the cost of transportation.

5. Conclusions

The results of the present work suggest that the carbon sequestration capacity of serpentinized harzburgites can be substantially enhanced by the ball milling process. CO_2-TPD experiments indicated that the optimum ball milling conditions for this ultramafic lithology are 16 h of wet ball milling with 50 wt% ethanol as process control agent, leading to an increase of CO_2 uptake by a factor of 4.5 compared to the unmilled sample. The same experiments also revealed that ball milling promotes the formation of more strongly bound carbonate-type species during CO_2 chemisorption, thus ensuring the safe storage of CO_2 over the long term. PXRD, SEM and TEM/HRTEM studies indicated that the enhancement of CO_2 uptake is mainly attributed to the reduction of particle size to the nanoscale range, as well as to the structural disordering of the constituent Mg-silicate minerals. However, ball milling longer than 16 h results in a lower specific surface area and subsequently in a reduced CO_2 uptake, mainly due to the increased degree of agglomeration after many hours of ball milling. The existence of significant volumes of serpentinized peridotites on almost every continent, in combination with the simplicity of the ball milling process, suggest that the enhancement of the carbon sequestration capacity of similar ultramafic lithologies by this method could possibly contribute to the mitigation of atmospheric CO_2 concentrations in the future.

Acknowledgements

This work was carried out in the context of the CO2NOR Project. This project has received funding from the European Union's Horizon 2020 research and innovation programme under the Marie Sklodowska-Curie grant agreement No 654091. We also thank Prof. K. Hatzipanagiotou from the Department of Geology of the University of Patras (Greece) for the preparation of the thin sections used for the petrographic analysis.

References

Balaz, P., Turianicova, E., Fabian, M., Kleiv, R.A., Briancin, J., Obut, A., 2008. Structural changes in olivine (Mg, $Fe_)2Si_O4$ mechanically activated in high-energy mills. Int. J. Miner. Process. 88 (1–2), 1–6.

Balucan, R.D., Dlugogorski, B.Z., 2013. Thermal activation of antigorite for mineralization of CO_2. Environ. Sci. Technol. 47, 182–190.

Batanova, V., Sobolev, A., 2000. Compositional heterogeneity in subduction-related mantle peridotites, Troodos massif, Cyprus. Geology 28, 55–58.

Bobicki, E.R., Liu, Q., Xu, Z., Zeng, H., 2012. Carbon capture and storage using alkaline industrial wastes. Prog. Energy Combust. Sci. 38, 302–320.

Bodénan, F., Bourgeois, F., Petiot, C., Augé, T., Bonfils, B., Julcour-Lebigue, C., Guyot, F., Boukary, A., Tremosa, J., Lassin, A., Gaucher, E.C., Chiquet, P., 2014. Ex situ mineral carbonation for CO_2 mitigation: Evaluation of mining waste resources, aqueous carbonation processability and life cycle assessment (Carmex project). Miner. Eng. 59, 52–63.

Ciais, P., Gasser, T., Paris, J.D., Caldeira, K., Raupach, M.R., Canadell, J.G., Patwardhan, A., Friedlingstein, P., Piao, S.L., Gitz, V., 2013. Attributing the increase in atmospheric CO_2 to emitters and absorbers. Nat. Climate Change 3, 926–930.

Costa, C.N., Anastasiadou, T., Efstathiou, A.M., 2000. The selective catalytic reduction of nitric oxide with methane over La_2O_3–CaO systems: synergistic effects and surface reactivity studies of NO, CH_4, O_2, and CO_2 by transient techniques. J. Catal. 194 (2), 250–265.

Declercq, J., Bosc, O., Oelkers, E.H., 2013. Do organic ligands affect forsterite dissolution rates? Appl. Geochem. 39, 69–77.

Dlugogorski, B.Z., Balucan, R.D., 2014. Dehydroxylation of serpentine minerals: Implications for mineral carbonation. Renew. Sustain. Energy Rev. 31, 353–367.

Efstathiou, A.M., Bennett, C.O., 1990. Enthalpy and entropy of H_2 adsorption on Rh/Al_2O_3 measured by temperature-programmed desorption. J. Catal. 124, 116–126.

Gass, I.G., Smewing, J.D., 1973. Intrusion, extrusion, and metamorphism at constructive margins; Evidence from the Troodos massif, Cyprus. Nature 242, 26–29.

Gerdemann, S.J., O'Connor, W.K., Dahlin, D.C., Panner, L.R., Rush, H., 2007. Ex situ aqueous mineral carbonation. Environ. Sci. Technol. 41 (2007), 2587–2593.

Gislason, S.R., Oelkers, E.H., 2014. Carbon storage in basalt. Science 344, 373.

Haug, A.H., Kleiv, R.A., Munz, I.A., 2010. Investigating dissolution of mechanically actibated olivine for carbonation purposes. Appl. Geochem. 25, 1547–1563.

IPCC, 2005. In: Metz, B., Davidson, O., de Coninck, H.C., Loos, M., Meyer, L.A., (Eds.), Carbon Dioxide Capture and Storage. Cambridge University Press, Cambridge, United Kingdom and New York, NY, USA, pp. 442.

Keeling, C.D., Whorf, T.P., Wahlen, M., van der Plicht, J., 1995. Interannual extremes in the rate of rise of atmospheric carbon dioxide since 1980. Nature 75, 666–670.

Kemache, N., Pasquier, L.-C., Mouedhen, I., Cecchi, E., Blais, J.-F., Mercier, G., 2016. Aqueous mineral carbonation of serpentinite on a pilot scale: The effect of liquid recirculation on CO_2 sequestration and carbonate precipitation. Appl. Geochem. 67, 21–29.

Kleiv, R.A., Thornhill, M., 2006. Mechanical activation of olivine. Miner. Eng. 19, 340–347.

Kleiv, R.A., Thornhill, M., 2016. The effect of mechanical activation in the production of olivine surface area. Miner. Eng. 89, 19–23.

Kuo, C., Lindberg, C., Thomson, D.J., 1990. Coherence established between atmospheric carbon dioxide and global temperature. Nature 343, 709–714.

Lackner, K.S., Wendt, C.H., Butt, D.P., Joyce, E.L., Sharp, D.H., 1995. Carbon dioxide disposal in carbonate minerals. Energy 20, 1153–1170.

Li, J., Hitch, M., 2016a. Characterization of the microstructure of mechanically-activated olivine using X-ray diffraction pattern analysis. Miner. Eng. 86, 24–33.

Li, J., Hitch, M., 2016b. Mechanical activation of ultramafic mine waste rock in dry condition for enhanced mineral carbonation. Miner. Eng. 95, 1–4.

Li, J., Hitch, M., 2016c. Carbon dioxide adsorption isotherm study on mine waste for integrated CO_2 capture and sequestration processes. Powder Technol. 291, 408–413.

Li, J., Hitch, M., 2017a. Ultra-fine grinding and mechanical activation of mine waste rock using a planetary mill for mineral carbonation. Int. J. Miner. Process. 158, 18–26.

Li, J., Hitch, M., 2017b. Structural and chemical changes in mine waste mechanically-activated in various milling environments. Powder Technol. 308, 13–19.

Matter, J.M., Kelemen, P.B., 2009. Permanent storage of carbon dioxide in geological reservoirs by mineral carbonation. Nat. Geosci. 2, 837–841.

Matter, J.M., Stute, M., Snæbjörnsdottir, S.Ó., Oelkers, E.H., Gislason, S.R., Aradottir, E.S., Sigfusson, B., Gunnarsson, I., Sigurdardottir, H., Gunnlaugsson, E., Axelsson, G., Alfredsson, H.A., Wolff-Boenisch, D., Mesfin, K., de la Reguera Taya, D.F., Hall, J., Dideriksen, K., Broecker, W.S., 2016. Rapid carbon mineralization for permanent disposal of anthropogenic carbon dioxide emissions. Science 352 (6291), 1312–1314.

Michael, K., Golab, A., Shulakova, V., Ennis-King, J., Allinson, G., Sharma, S., Aiken, T., 2010. Geological storage of CO_2 in saline aquifers - A review of the experience from existing storage operations. Int. J. Greenhouse Gas Control 4, 659–667.

Mukasa, S.B., Ludden, J.N., 1987. Uranium–lead ages of plagiogranites from the Troodos ophiolite, Cyprus, and their tectonic significance. Geology 1, 825–828.

Munz, I.A., Brandvoll, Ø., Haug, T.A., Iden, K., Smeets, R., Kihle, J., Johansen, H., 2012. Mechanisms and rates of plagioclase carbonation reactions. Geochim. Cosmochim. Acta 77, 27–51.

NOAA-ESRL, 2017. Trends in Atmospheric Carbon Dioxide - Earth System Research Laboratory. Global Monitoring Division – NOAA. http://www.esrl.noaa.gov/gmd/ccgg/trends/.

O'Connor, W.K., Dahlin, D.C., Rush, G.E., Gerdemann, S.J., Penner, L.R., Nilsen, D.N., 2005. Aqueous mineral carbonation: mineral availability, pretreatment, reaction parametrics and process studies. Albany Research Center DOE/ARC-TR-04-002: Albany, OR, USA.

Oelkers, E.H., Gislason, S.R., Matter, J., 2008. Mineral carbonation of CO_2. Elements 4, 333–337.

Olajire, A.A., 2013. A review of mineral carbonation technology in sequestration of CO_2. J. Petrol. Sci. Eng. 109, 364–392.

Pearce, J.A., Robinson, P.T., 2010. The Troodos ophiolitic complex probably formed in a subduction initiation, slab edge setting. Gondwana Res. 18, 60–81.

Power, I.M., Harrison, A.L., Dipple, G.M., Wilson, S.A., Kelemen, P.B., Hitch, M., Southam, G., 2013. Carbon mineralization: from natural analogues to engineered systems. Rev. Mineral. Geochem. 77, 305–360.

Rigopoulos, I., Petallidou, K.C., Vasiliades, M.A., Delimitis, A., Ioannou, I., Efstathiou, A.M., Kyratsi, Th., 2015a. Carbon dioxide storage in olivine basalts: effect of ball milling process. Powder Technol. 273, 220–229.

Rigopoulos, I., Vasiliades, M.A., Petallidou, K.C., Ioannou, I., Efstathiou, A.M., Kyratsi, Th., 2015b. A method to enhance the CO_2 storage capacity of pyroxenitic rocks. Greenhouse Gas. Sci. Technol. 5, 1–14.

Rigopoulos, I., Vasiliades, M.A., Ioannou, I., Efstathiou, A.M., Godelitsas, A., Kyratsi, Th., 2016a. Enhancing the rate of ex situ mineral carbonation in dunites. Adv. Powder Technol. 27, 360–371.

Rigopoulos, I., Petallidou, K.C., Vasiliades, M.A., Delimitis, A., Ioannou, I., Efstathiou, A.M., Kyratsi, Th., 2016b. On the potential use of quarry waste material for CO_2 sequestration. J. CO_2 Util. 16, 361–370.

Rigopoulos, I., Harrison, A.L., Delimitis, A., Ioannou, I., Efstathiou, A.M., Kyratsi, Th., Oelkers, E.H., 2017. Enhanced weathering of peridotites and basalts in seawater. Appl. Geochem. http://dx.doi.org/10.1016/j.apgeochem.2017.11.001.

Robertson, A.H.F., 2002. Overview of the genesis and emplacement of Mesozoic ophiolites in the Eastern Mediterranean Tethyan region. Lithos 65, 1–67.

Robinson, P.T., Malpas, J., 1990. The troodos ophiolite of Cyprus: new perspectives on its origin and emplacement. In: Malpas, J., Moores, E.M., Panayiotou, A., Xenophontos, C., (Eds.), Ophiolites: Oceanic Crustal Analogues. Cyprus Geol. Surv. Dept., Nicosia, pp. 13–36.

Sanna, A., Uibu, M., Caramanna, G., Kuusik, R., Maroto-Valer, M., 2014. A review of mineral carbonation technologies to sequester CO_2. Chem. Soc. Rev. 43, 8049–8080.

Sawyer, 1972. Man-made carbon dioxide and the "greenhouse" effect. Nature 239, 23–26.

Seifritz, W., 1990. CO_2 disposal by means of silicates. Nature 345, 486–490.

Siegenthaler, U., Oeschger, H., 1987. Biospheric CO_2 emissions during the past 200 years reconstructed by deconvolution of ice core data. Tellus 39B, 140–154.

Solomon, S., Plattner, G.-K., Knutti, R., Friedlingstein, P., 2009. Irreversible climate change due to carbon dioxide emissions. PNAS 106 (6), 1704–1709.

Turianicová, E., Baláž, P., Tuček, L., Zorkovská, A., Zeleňák, V., Németh, Z., Šatka, A., Kováč, J., 2013. A comparison of the reactivity of activated and non-activated olivine with CO_2. Int. J. Miner. Process. 123, 73–77.

UNFCCC, 2016. The 2015 Paris Climate Change Conference: COP21. Vol. 99, pp. 97–104.

Wilson, S.A., Harrison, A.L., Dipple, G.M., Power, I.M., Barker, S.L.L., Ulrich Mayer, K., Fallon, S.J., Raudsepp, M., Southam, G., 2014. Offsetting of CO_2 emissions by air capture in mine tailings at the Mount Keith Nickel Mine, Western Australia: Rates, controls and prospects for carbon neutral mining. Int. J. Greenhouse Gas Control 25, 121–140.